Journal of Applied Sciences

ISSN 1812-5654

science alert

ANSInet
an open access publisher
http://ansinet.com

Journal of Applied Sciences 9 (16): 2925-2932, 2009
ISSN 1812-5654

Experimental and Numerical Analysis for Hydroforming of Ti6Al4V Alloy Used in Aerospace, Assisted by Floating Disk

H. Nezami Esfahlan, Sh. Abbasnejad Dizaji and F. Djavanroodi
Department of Mechanical Engineering, Iran University of Science and Technology, Tehran, Iran

Abstract: As an advanced technology of sheet metal forming, Hydromechanical Deep Drawing (HDD) is being used increasingly in the sheet metal forming of common materials like aluminum, steel and titanium alloys. In this study, a new method of deep drawing assisted by floating disk is investigated in details for Ti6Al4V both in experimental and simulation. The effects of process parameters on cylindrical cups of Ti6Al4V are discussed. Working pressure curves, which guarantee sound Ti6Al4V work pieces, was founded by series of experimental results. Thickness variation, wrinkling and fracture modes are discussed. Finite element method model by ABAQUSE 6.5 was used to analyze this hydroforming process. NADDRG, Hill-Swift and Aly El-Domiaty theoretical FLD models were used to specify fracture initiation and compared with each other. According to comparisons there is a good agreement between experimental and numerical results.

Key words: Titanium alloys, hydromechanical deep drawing, floating disk, experimental results, FEM model

INTRODUCTION

Hydroforming or hydraulic forming has been one of the fundamental sheet metal forming processes for quite along time. The female die in the conventional deep drawing process is replaced by hydromechanical deep drawing process is placed by a counter pressure created from a fluid. A rubber diaphragm prevents leakage and punch determines the final shape of the work piece. The fluid pressure acts as blank holder and prevents wrinkles (Zhang, 1999). There were so many methods for hydroforming as Zhang *et al*. (2003) have showed some of them they also investigated about the quality of the formed parts and showed that it can be influenced by the material properties. Anisotropy has more influence on the parts shape and the thickness distribution than in the conventional deep drawing process as the drawing ratio in the HDD process is usually very high, but hydroforming assisted by floating disk, is a new method that has been investigated in this study. Because of floating disk's rigidity it eliminates wrinkles and permits the process to be done in lower hydraulic pressures. Compared with the conventional deep drawing process, the limit drawing ratio can be increased from 1.8 to 2.8, the tool costs can be reduced remarkably as only one tool half (the punch) is used, the female die is replaced with the chamber fluid, only the punch needs to be varied when drawing parts with different shapes and dimensions (Kandil, 2003; Zhang *et al*., 2003). Shulkin *et al*. (2000) found an appropriate relationship for pressure versus punch stroke so as to maintain the thickness unchanged for the hydro-forming of axisymmetric shapes. They also derived a theoretical relationship for wrinkling in axisymmetric hydroforming. Choi *et al*. (2007) considered normal anisotropy in the analysis of the instability in hydroforming. In this study, a simple method, to determine optimal pressure curve for the sheet hydroforming process, based on the Theoretical analysis has been proposed and the corresponding experiments are carried out to verify the recommended pressure curve. To determine optimal pressure curve for sheet hydroforming, Shim and Yang (2005) has introduced a good method. Hill has developed an anisotropic yield function to apply anisotropic characteristic of materials in sheet metals which Holmberg *et al*. (2004) utilized it very carefully to determine the anisotropic characteristics of the material. Lang *et al*. (2004, 2005) investigated about hydrodynamic deep drawing, advantages and disadvantages of Minus Pre-Bulging (MPB) and Plus Pre-Bulging (PPB) and failure modes. According the results of comparing between FLD diagrams, the NADDRG model (Slota and Spisak, 2005), El-Domiaty model (El-Domiaty, 1992) and Hill-Swift model (Bleck *et al*., 1998) were chosen to predict fracture initiation and compared with each other. Using numerical simulation, this process can be studied and developed systemically, which will be very helpful to the practical application in industry especially metal forming and create

Corresponding Author: Sh. Abbasnejad Dizaji, Department of Mechanical Engineering, Iran University of Science and Technology, Tehran, Iran Fax: +984412353690

the knowledge base for the so called virtual design or virtual prototyping, which are both based on the FEM (Narayanasamy *et al*., 2006; Guan *et al*., 2006).

HYDROFORMING TEST

In order to study the process, material characteristics were obtained experimentally. Beside all methods introduced till now, hydroforming assisted by floating disk, is a new method that can simplify the tools used for hydroforming and decrease cost of process.

Material: The test material is Ti6Al4V titanium alloy (MILT 9046_Ty1_Comp C_HT N-3387) with the thickness of 1.08 mm. Table1 shows the properties for this material obtained from uniaxial tensile test based on ASTM E8 standard and anisotropic characteristics (r-values) obtained according ASTM E517 standard.

Ti6Al4V is the most widely used titanium alloy. It combines attractive properties with inherent workability which allows it to be fabricated into complex shapes. It is used for aircraft gas turbine disks and blades, aircraft hydraulic systems, air engine components, rockets, guided missiles, space craft and other applications requiring strength and temperature up to 315°C. Ti6Al4V is 30% stronger than steel, but is nearly 50% lighter. Ti6Al4V is 60% heavier than aluminum, but twice as strong. Ti6Al4V at room temperature is a hard to form material because of high-strength and hcp structure.

Tools: The essential parts of the tool for hydroforming process include a punch, a blank holder, a pressure chamber, a rubber diaphragm and a floating disk as a die (Fig. 1). Diaphragm at the bottom can move up and down or form by pressure of viscous medium in chamber. Blank is placed between blank holder and flouting die. Blank Holding Force (BHF) due to pressure of chamber and area of floating disk, can press blank tightly to blank holder. As the punch moves down, forming the cup, a control valve regulates the liquid flow. The pressure curve for successful forming has pre-determined theoretically and corrected experimentally.

All the experiments were carried out using a 250 t hydraulic double-action press. Figure 2 shows a picture of the whole equipment and Table 2 shows the dimensions of the tools used for this process.

This study emphasizes the use of numerical simulation for analyzing the deformation process of the blank and for providing the effective methods to prevent failures during process.

Procedure: Initially, the hydraulic fluid is filled up to the shoulder of the container and the rubber diaphragm inserted in place then locked and sealed by locking disk. The blank is lubricated by grease in both sides then

Table 1: Properties of the material (Ti6Al4V)

	Angle to rolling direction		
Parameters	0°	45°	90°
Density (g cm^{-3})	4.43		
Poisson's ratio	0.342		
Elastic modulus (GPa)	22.5	22.0	22.5
Yielding stress (MPa)	544	558	571
Ultimate tensile stress (MPa)	632	607	629
Total elongation (%)	30.7	27.2	28.0
Anisotropy factor (R_{x°)	2.4644	4.1218	3.8292
θ	49.855°	49.105°	
Anisotropy factor (R)	3.6343		
ΔR	-0.975		
Strain hardening exponent (n)	0.151	0.134	0.167
Hardening coef. k (MPa)	975	912.5	1022
Strain rate sensitivity (m)	0.02	0.02	0.02
Change of strain rate with strain	4.1	4.1	4.1

Table 2: Tool dimensions

Parameters	Values
Punch diameter d (mm)	40
Inside die (disk) diameter d_d (mm)	43.5
Punch nose radius r_p (mm)	5, 10, 15
Die entrance radius r_{die} (mm)	5
Inside blank holder diameter d_c (mm)	40.2
Blank holder entrance radius R_c (mm)	2

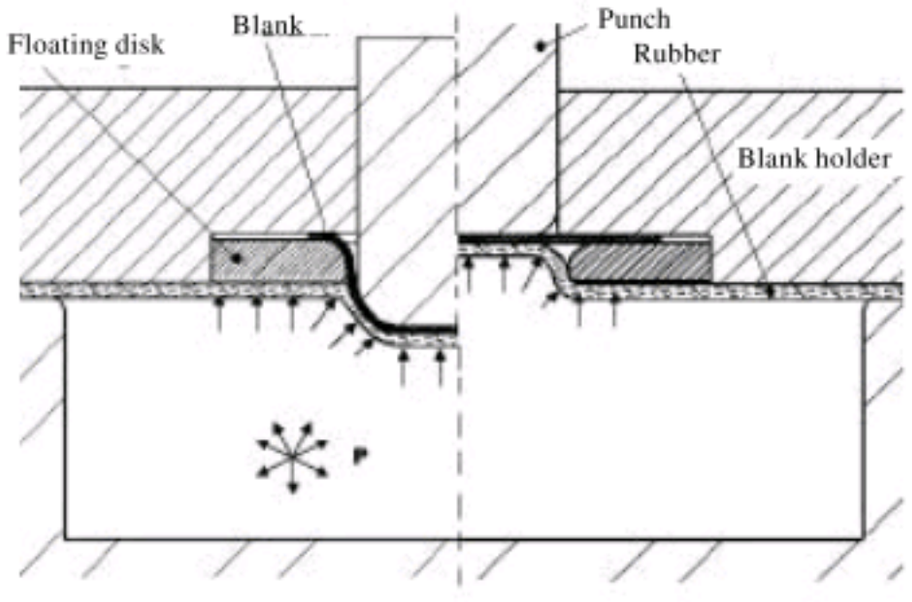

Fig. 1: The hydroforming process assisted by floating disk

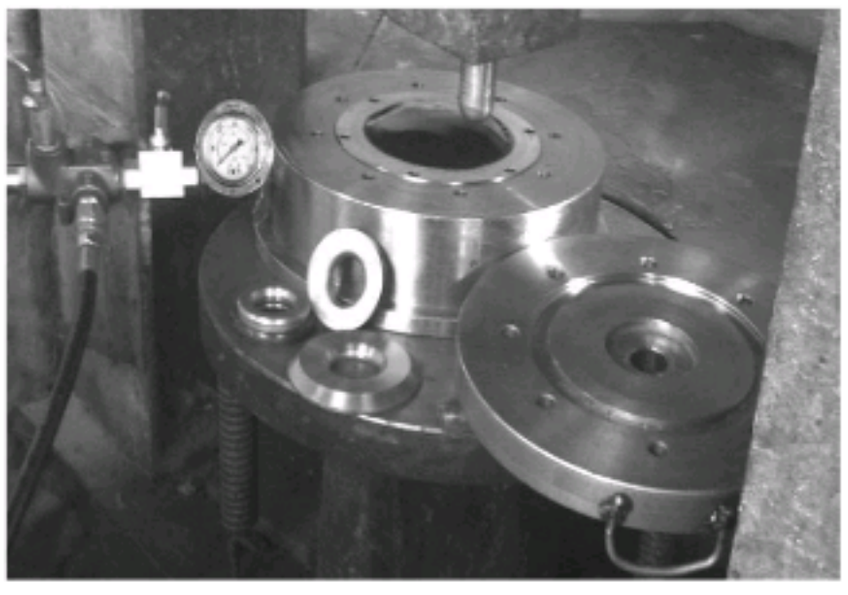

Fig. 2: Hydraulic press and die

placed between disk and blank holder and centralized in the place. The blank holder diameter is selected according to blank diameter and the Blank Holder Force (BHF) needed for process. The blank holder is then placed on top of the container and eight bolts are screwed on to keep it tight, it even helps sealing of rubber diaphragm in this state. The punch, which is fastened to the press ram, is lowered through the central hole in the blank holder up to 3 mm of the blank. The hydraulic valve is now opened and the pressure in the cavity is gradually raised up to a specified value to form the blank upward in reverse direction (PPB). The punch is advanced down to draw the cup at the specified speed. The press ram will prevent retraction of the punch when the cavity is pressurized. Whilst the cup is being drawn the fluid pressure will begin to increase, but this is regulated and settled by the pressure relief valve, thus the excess fluid from the cavity is returned to the sump. At the end of drawing the press ram is stopped and the fluid pressure in the cavities released. Once the cavities depressurized, the punch is withdrawn. There after the bolts are unscrewed and the cover plate is removed, the cup that has been formed remains on the diaphragm and is removed: sometimes the cup sticks to the punch and has to be tapped out. The minimum chamber pressure to prevent wrinkling versus punch stroke diagram can be calculated by Eq. 1, which is approved by Shim and Yang (2005) and α is correction factor of punch shape. In this new method, a modified version of equation given by Shim and Yang (2005) due to existence of floating disk, was used to get punch force of hydroforming by Eq. 2.

$$P_s > \frac{4d.t.\sigma_y}{(D_d^2 - d_p^2)\sqrt{3}}\alpha \quad (1)$$

$$F_{punch}/\pi d_p t = 1.1\sigma_m Ln\beta + \frac{\mu P_s}{4} + (\beta^2 - 1)\left(\frac{1}{\beta} + 1\right)\frac{d_p}{t} + \frac{P_s d_p}{4t} + \sigma_2\left(\frac{t}{2r_d}\right) - p_r \quad (2)$$

RESULTS AND DISCUSSION

The results from the experiments as mentioned above, are analyzed and discussed as follows:

Experimental: At first stage after installation of sheet in its position by means of grease and floating disk to form this sheet, pressure of chamber should be regulated precisely versus punch stroke. To obtain pressure curve, a simple method is introduced by Shim and Yang (2005). According to this method, we can calculate the initial pressure from flange and punch forces. This procedure leads to initial pressure equal to 15.5 MPa. Figure 3 shows chamber pressure versus punch stroke curves using a punch with a nose radius of 20, 10 and 5 mm and Fig. 4a-c shows their punch force versus punch stroke curves taken by load sensor in Limit Drawing Ratio (LDR) of 2.25, respectively.

As shown in Fig. 3a, initial pressure for this alloy is about 165 bar, so Shim's method for obtaining initial pressure can be applied to this ductile alloy. Pressure in the die cavity can be divided into 5 zones.

- Zone 1 is pre-bulging where blank will be bulged 3 mm in reverse direction
- Zone 2 is where the initial pressure is applied and it is very important stage which can be calculated theoretically as mentioned
- Zone 3 is where pressure increases with sharp slope in comparison with other zones
- Zone 4 is control zone
- Zone 5 is where finally liquid pressure decreases rapidly and is released because the entire flange has been pulled into the die cavity

As punch radii effect, there is just big different in initial pressure; decreasing punch radii leads to increasing in initial pressure (Fig. 3a-c), but in the other zones, diagrams are same approximately, so effect of this parameter is only in second zone.

Figure 5 shows the blank holder force versus punch stroke curve taken by the formula in Limit Drawing Ratio (LDR) of 2.25.

Simulation: To explore the deformation secrets that cannot be observed directly in experiments, FEM by ABAQUSE 6.5 was used. The commercial explicit finite element code was used. Due to the symmetric character of the forming, only a quarter of the model was used. All tools were modeled using an analytical rigid and the material were modeled using S4R (A 4-node quadrilateral in-plane general-purpose shell, reduced integration) elements for fracture prediction and C3D8R (An 8 node linear brick, reduced integration) elements for modeling anisotropic effects in sheets. Mesh size is 0.5 mm and penalty contact interfaces were used to enforce the intermittent contact and the sliding boundary condition between the blank and the tooling elements. The material parameters used for the blank derived from the uniaxial tensile test. Anisotropy options calculated according ASTM-E517 and r_0, r_{45} and r_{90} were used to calculate F, G, H, N, L and M which are material constants in Hill 48 yield function.

Hill's potential function is an extension from the Mises function and can be expressed as:

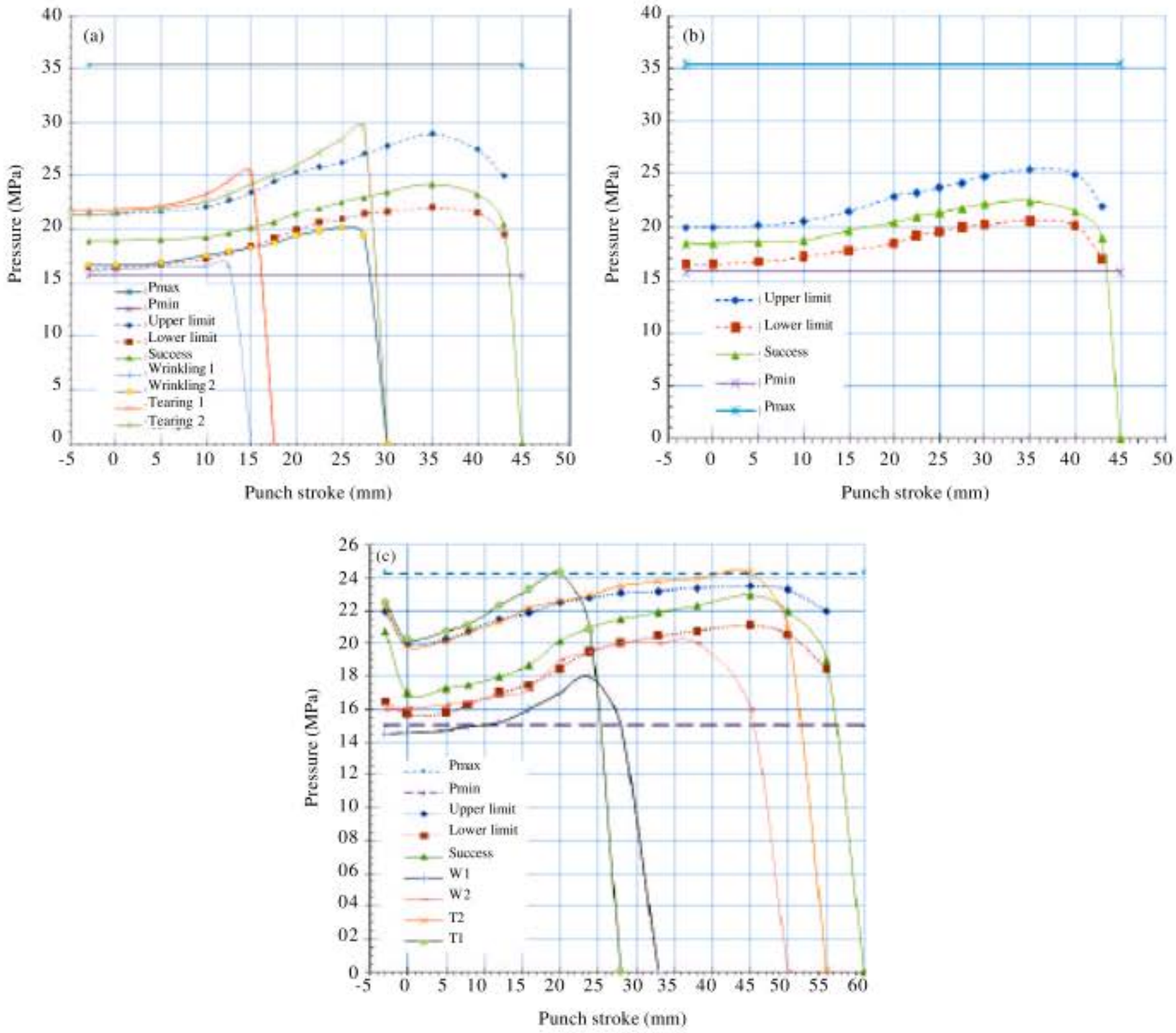

Fig. 3: Pressure-punch stroke curves for Ti6Al4V with LDR = 2.25, (a) punch radii = 5, (b) punch radii = 10 and (c) punch radii = 20

$$f(\sigma)=\sqrt{F(\sigma_{22}-\sigma_{33})^2+G(\sigma_{33}-\sigma_{11})^2+H(\sigma_{11}-\sigma_{22})^2+2L\sigma_{23}^{\ 2}+2M\sigma_{31}^{\ 2}+2L\sigma_{12}^{\ 2}} \quad (3)$$

where, σ_{ij} denotes the stress components. Material constants can be expressed in terms of six yield stress ratios R_{11}, R_{22}, R_{33}, R_{12}, R_{13} and R_{23} according to Eq. 4.

In sheet metal forming, anisotropic material data is defined in terms of ratios of width strain to thickness strain commonly. The stress ratios can then be defined as Eq. 5.

Then these calculated ratios can be interred to software directly to simulate anisotropic material based on Hill criteria in FEM.

$$F=\frac{1}{2}\left(\frac{1}{R_{22}^{\ 2}}+\frac{1}{R_{33}^{\ 2}}-\frac{1}{R_{11}^{\ 2}}\right),\ G=\frac{1}{2}\left(\frac{1}{R_{11}^{\ 2}}+\frac{1}{R_{33}^{\ 2}}-\frac{1}{R_{22}^{\ 2}}\right),$$
$$H=\frac{1}{2}\left(\frac{1}{R_{11}^{\ 2}}+\frac{1}{R_{22}^{\ 2}}-\frac{1}{R_{33}^{\ 2}}\right),\ L=\frac{3}{2R_{23}^{\ 2}},\ M=\frac{3}{2R_{13}^{\ 2}},\ N=\frac{3}{2R_{12}^{\ 2}} \quad (4)$$

$$R_{11}=R_{13}=R_{23}=1,\quad R_{22}=\sqrt{\frac{r_{90}(r_0+1)}{r_0(r_{90}+1)}}$$
$$R_{33}=\sqrt{\frac{r_{90}(r_0+1)}{r_{90}+r_0}},\quad R_{12}=\sqrt{\frac{3r_{90}(r_0+1)}{(2r_{45}+1)(r_{90}+r_0)}} \quad (5)$$

To determine location of fracture in FEM model, FLD data applied to software indirectly based on NADDRG, Hill-Swift and El-Domiaty model by user subroutine.

The NADDRG model: For simplifying the experimental and theoretical determination of the FLD and utilizing the FLD more easily in the press workshop, the North American Deep Drawing Research Group (NADDRG) introduced an empirical equation. According to this model FLD is composed of two lines through the point Fld_0 in the plane-strain state. The slope of the lines located on the left and right side of FLD are about 45 and 20°. The equation is:

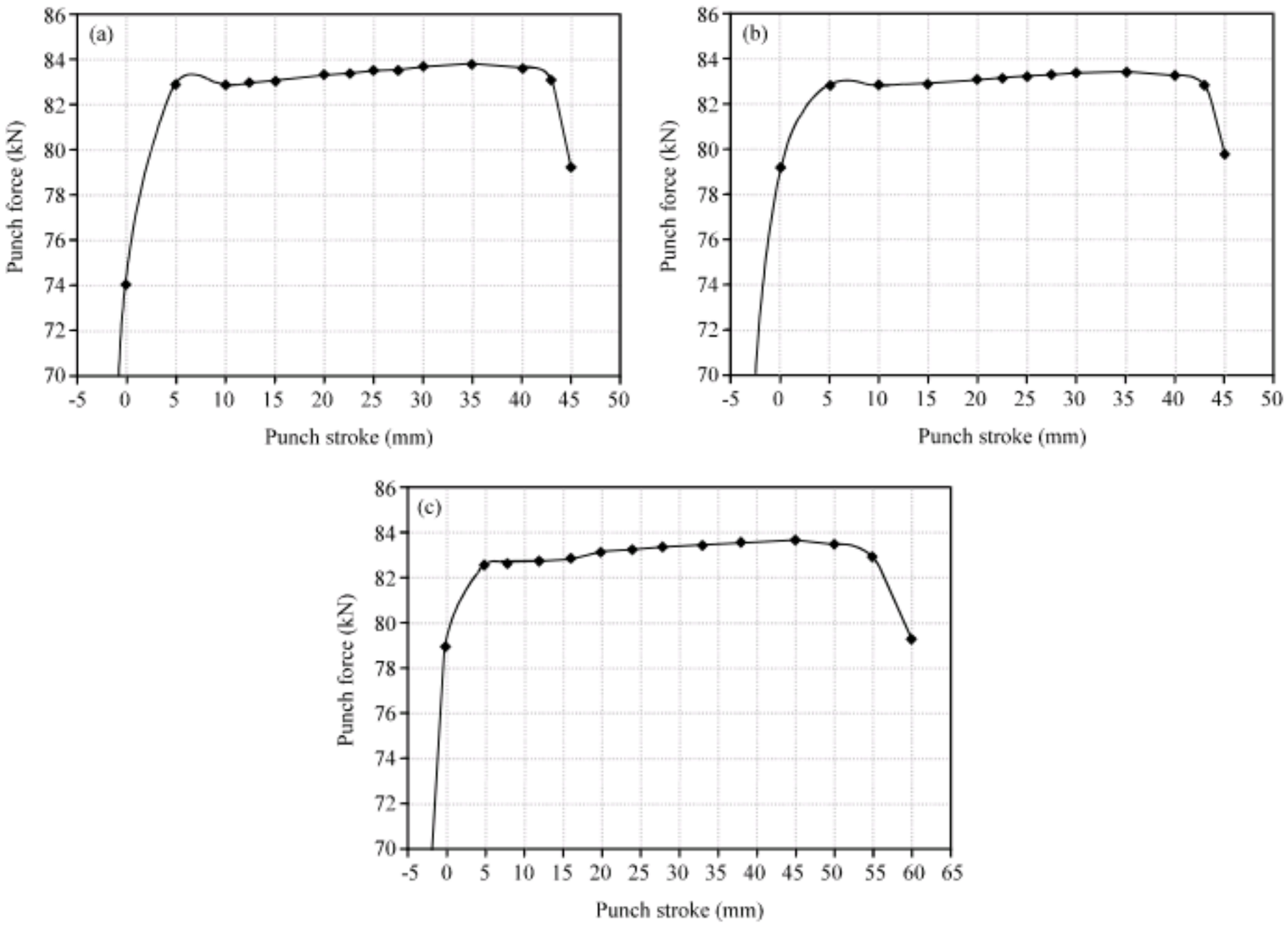

Fig. 4: Punch force-punch stroke curve for Ti6Al4V with LDR = 2.25, (a) punch radii = 5, (b) punch radii = 10 and (c) punch radii = 20

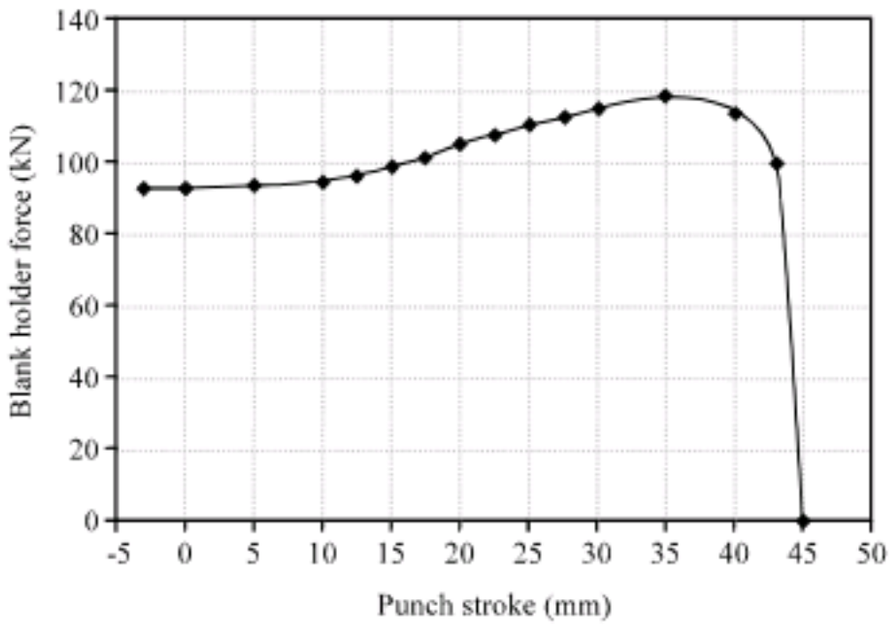

Fig. 5: Blank holder force versus punch stroke curves for Ti6Al4V for punch radii = 5

$$e_{10} = (23.3 + 14.1t)\frac{n}{0.21} \quad (6)$$

The Hill-Swift model: It has been proven that a good simulation of the forming limit strains can be given on the basis of the Swift diffuse instability theory and the Hill localized instability theory and where Swift's and Hill's theories are used to calculate the forming limit strains on the left and the right side, respectively, of the FLD. According to Swift's and Hill's criterion, the formula calculating the forming-limit strains can be written as follows, with $\alpha = \sigma_2/\sigma_1$,

For $\varepsilon_2<0$:

$$\varepsilon_{j1} = \frac{1+(1-\alpha)R}{1+\alpha}n \quad (7)$$

$$\varepsilon_{j2} = \frac{\alpha+(1-\alpha)R}{1+\alpha}n \quad (8)$$

For $\varepsilon_2>0$:

$$\varepsilon_{f1} = \frac{[1+R(1-\alpha)][1-\frac{2R}{1+R}\alpha+\alpha^2]}{(1+\alpha)(1+R)[1-\frac{1+4R+2R^2}{(1+R)^2}\alpha+\alpha^2]} \quad (9)$$

$$\varepsilon_{f2} = \frac{[(1+R)\alpha-R][1-\frac{2R}{1+R}\alpha+\alpha^2]}{(1+\alpha)(1+R)[1-\frac{1+4R+2R^2}{(1+R)^2}\alpha+\alpha^2]} \quad (10)$$

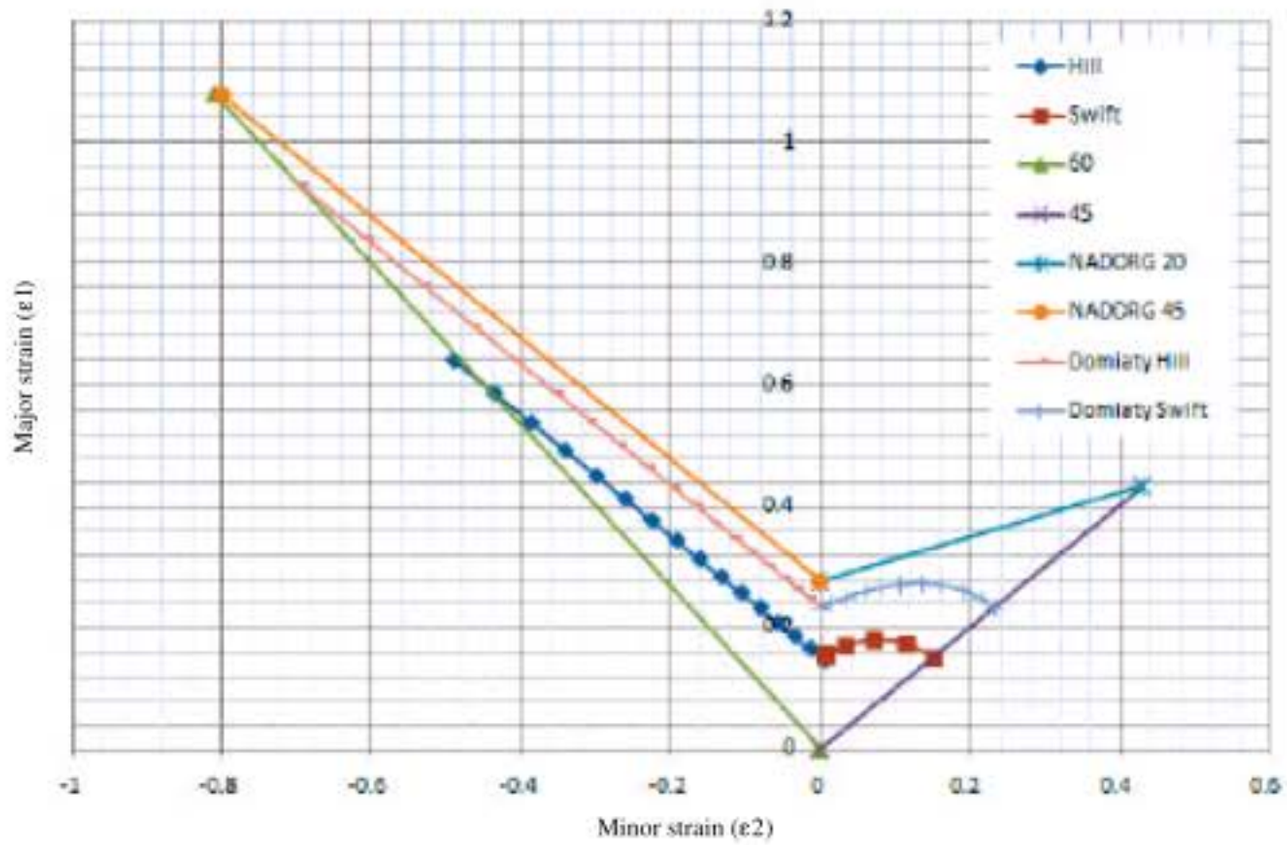

Fig. 6: FLD diagrams

The El-Domiaty model: The standard tension tests were carried out to determine the strain hardening exponent, n and strain rate sensitivity exponent, m.

The effective limiting strain $\bar{\varepsilon}$ has been determined according to Conrad (x) as follows:

$$\bar{\varepsilon} = (n + m\dot{\gamma})Z \tag{11}$$

$$\dot{\gamma} = \frac{dLn\bar{\varepsilon}}{dLn\varepsilon} \tag{12}$$

$$Z = \frac{4(1-\alpha+\alpha^2)^{3/2}}{(1+\alpha)(4\alpha^2-7\alpha+4)} \tag{13}$$

$$Z = \frac{2(1-\alpha+\alpha^2)^{1/2}}{(1+\alpha)} \tag{14}$$

When the minor strain is negative, Z was taken according to Hill. But when the minor strain is positive the critical sub tangent Z was taken according to Swift. From the plasticity equations, the strain ratio $\beta = \varepsilon_2/\varepsilon_1$ is given by:

$$\beta = \frac{2\alpha-1}{2-\alpha} \tag{15}$$

$$\varepsilon_1 = \frac{\bar{\varepsilon}}{2}\frac{(2-\alpha)}{\sqrt{1-\alpha+\alpha^2}} \tag{16}$$

$$\varepsilon_2 = \frac{\bar{\varepsilon}}{2}\frac{(2\alpha-1)}{\sqrt{1-\alpha+\alpha^2}} \tag{17}$$

Assuming proportional loading (linear strain path) i.e. β takes constant values varies from β = -0.5 (uniaxial tension), the forming limit diagram can be determined by using Eq.11, 12, 15, 16, 17 and 13 or 14. In Fig. 6, all FLD models have been shown.

Comparison: There were three kinds of wrinkling and three kinds of fracture modes, forming these sheets totally. Figure 7a shows three kinds of wrinkling in Ti6Al4V that they are usually result of low blank holder force or low chamber pressure in different phases of hydroforming. Ofcorse some other parameters like lubricants used between blank and blank holder or ironing process might solve wrinkling problems. Figure 7b shows prediction of these failure modes by the simulation; Also, Fig. 8a shows three kinds of fracture modes in this titanium alloy and Fig. 8b shows the fracture modes, type one and type two predicted by FEM simulation. All three kinds of fractures are results of higher chamber pressure and therefore higher blank holder force. In order to prevent wrinkling and fracture there should be an appropriate curve of chamber pressure.

Comparing three FLD diagrams in Fig. 6, El-Domiaty has better prediction than NADDRG and Hill-Swift model, so in titanium sheets forming, using the former model is suggested. Besides, it is obvious that used FEM model is a suitable tool to analyze hydroforming process and can predict both wrinkling and fracture in sheets if the FEM model be suitable and complete.

Figure 9a and b show the successfully drawn cup with its simulated model.

(a)

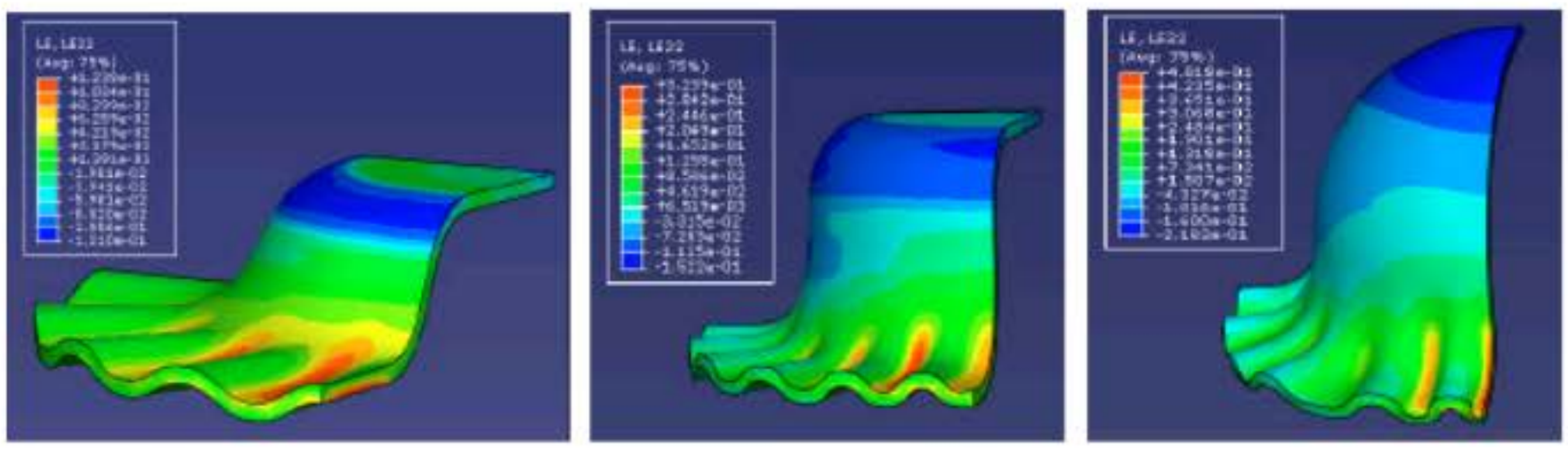

(b)

Fig. 7: Wrinkling modes in Ti6Al4V, (a) experimental and (b) simulation

(a)

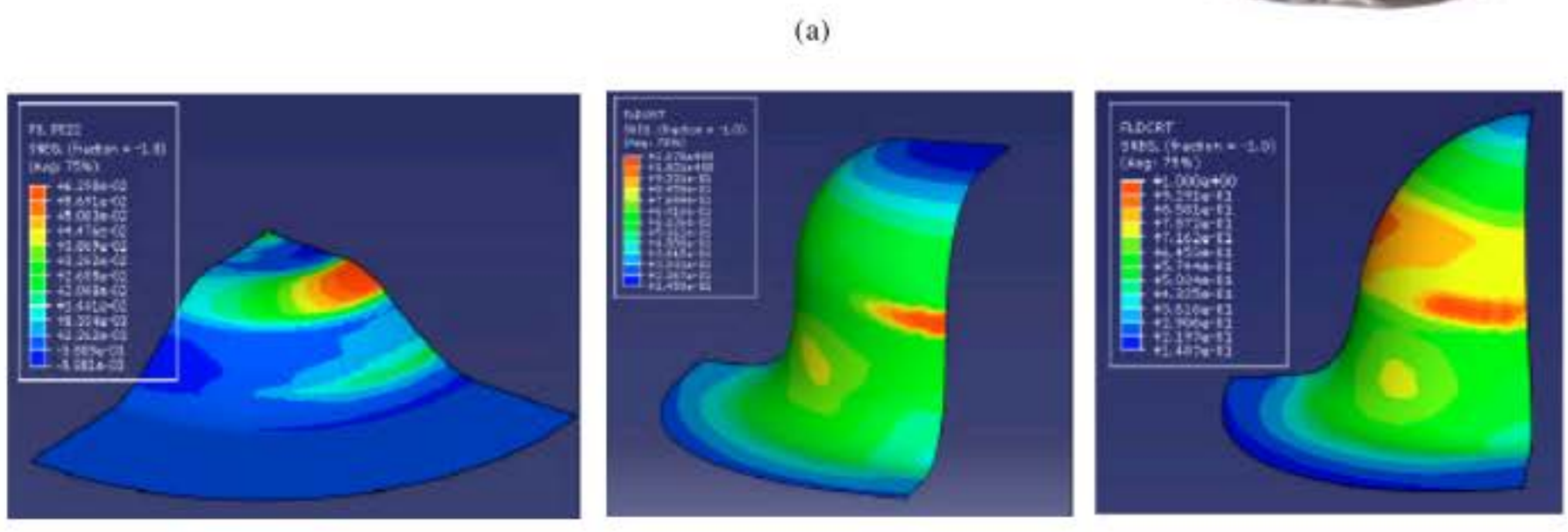

(b)

Fig. 8: Fracture modes in Ti6Al4V, (a) experimental and (b) simulation

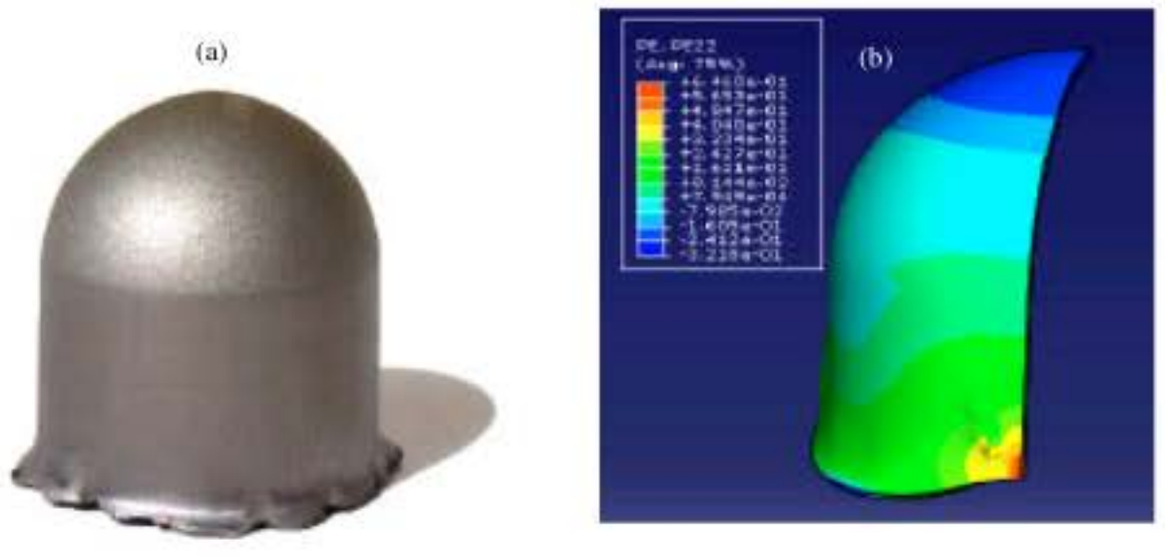

Fig. 9: Successfully drawn cup with its simulated model, (a) experimental and (b) simulation

CONCLUSION

This new method of hydromechanical deep drawing by floating disk assistance helps to form Ti alloys in lower scale of chamber pressure in comparison with the conventional hydroforming methods. It is due to the high capabilities of floating disk in preventing wrinkles and ironing capability. The negative points of this method are the higher surface roughness due to the contact of sheet with floating disk and needs to manufacture a floating disk with appropriate dimensions. Optimum pressure curve must be used to prevent wrinkling at lower pressures and cup fracture at unduly high pressures. Further investigations can be carried out to determine the effects of different punch and floating disk geometries, also neural network might lead to a better prediction of process parameters effect. By a little change on the die it can be used for hydro bulge testing of sheets.

ACKNOWLEDGMENTS

The authors would like to gratefully acknowledge NEZAMI Industry which helped them during tests and also Mr. M. Eskandarzade for his kindly suggestions.

REFERENCES

Bleck, W., Z. Deng, K. Papamantellos and C. Oliver, 1998. A comparative study of the forming-limit diagram models for sheet steels. J. Mater. Process. Technol., 83: 223-230.

Choi, H., M. Koc and J. Ni, 2007. Determination of optimal loading profiles in warm hydroforming of lightweight materials. J. Mater. Process. Technol., 190: 230-242.

El-Domiaty, A., 1992. The effect of strain, strain rate, and temperature on formability of Ti6Al4V alloy. J. Mater. Process. Technol., 32: 243-251.

Guan, Y., F. Pourboghrat and F. Barlat, 2006. Finite element modeling of tube hydroforming of polycrystalline aluminum alloy extrusions. J. Mater. Process. Technol., 22: 2366-2393.

Holmberg, S., B. Enquist and P. Thilderkvist, 2004. Evaluation of sheet metal formability by tensile tests. J. Mater. Process. Technol., 145: 72-83.

Kandil, A., 2003. An experimental study of hydroforming deep drawing. J. Mater. Process. Technol., 134: 70-80.

Lang, L., J. Danckert and K.B. Nielsen, 2004. Investigation into hydrodynamic deep drawing assisted by radial pressure Part I. Experimental observations of the forming process of aluminum alloy. J. Mater. Process. Technol., 148: 119-131.

Lang, L., J. Danckert and K.B. Nielsen, 2005. Investigation into hydrodynamic deep drawing assisted by radial pressure Part II. Numerical analysis of the drawing mechanism and the process parameters. J. Mater. Process. Technol., 166: 150-161.

Narayanasamy, R., R. Ponalagusamy and S. Raghuraman, 2006. The effect of strain rate sensitivity on theoretical prediction of limiting draw ratio for cylindrical cup drawing process. J. Mater. Process. Technol., 100: 131-141.

Shim, H. and D.Y. Yang, 2005. A simple method to determine pressure curve for sheet hydroforming and experimental verification. J. Mater. Process. Technol., 167: 169-177.

Shulkin, L.B., R.A. Posteraro, M.A. Ahmetoglu, G.L. Kinzel and T. Altan, 2000. Blank Holder Force (BHF) control in Viscous Pressure Forming (VPF) of sheet metal. J. Mater. Process. Technol., 98: 7-16.

Slota, J. and E. Spisak, 2005. Comparison of the Forming Limit Diagram (FLD) models for drawing quality of sheets. Metalurgia, 4: 249-253.

Zhang, S.H., 1999. Development of hydro-mechanical deep drawing. Int. J. Mech. Sci., 40: 1800-1807.

Zhang, S.H., M.R. Jensen, K.B. Nielsen, J. Danckert, L.H. Lang and D.C. Kang, 2003. Effect of anisotropy and prebulging on hydromechanical deep drawing of mild steel cups. J. Mater. Process. Technol., 142: 544-550.